Electronic Supplementary Material (ESI) for Nanoscale.
This journal is © The Royal Society of Chemistry 2021

# Supporting Information

## Electrocatalytically Inactive Copper Improves the Water Adsorption/Dissociation on $Ni_3S_2$ for Accelerated Alkaline and Neutral Hydrogen Evolution

*Lei Zhang,[a] Xiaorui Gao,[a]* Ying Zhu,[a] Acan Liu,[a] Huilong Dong, [a]* Dajun Wu,[a] Zhida Han,[a] Wei Wang,[b] Yong Fang,[a] Jie Zhang,[a] Zongkui Kou,[c] Bin Qian, [a]* and Tingting Wang,[d]**

1. **Note:** In the supporting information, Cu-$Ni_3S_2$ nanoparticles fabricated on the Ni foams pretreated in $CuCl_2$ solution for 0, 2, 4, 6, 8 and 10 min are denoted as CNS0, CNS2, CNS4, CNS6, CNS8 and CNS10, respectively.
2. **Computational methods**

All the first-principles calculations were performed by the Vienna ab initio simulation package (VASP).[1] The projected augmented wave (PAW)[2] was utilized for description of the ion-electron wave-function (at the ground state). The Perdew−Burke−Ernzerhof (PBE)[3] functional within the generalized gradient approximation (GGA) was employed for expression of electron exchange-correlation. The Grimme's method (DFT-D3)[4] was applied to include the weak van der Waals (vdW) interactions. Cutoff energy of 500 eV was chosen for the plane-wave basis set after testing. The iterative convergence of energy and force during optimization was set as $10^{-5}$ eV and 0.02 eV /Å, respectively.

The lattice parameter of bulk $Ni_3S_2$ (primitive cell) was calculated as 4.078 Å, in good accordance with the experimentally measured value (4.08 Å).[5] The gamma-centred Monkhorst–Pack scheme[6] was used for the sampling of Brillouin zone, with a K-point mesh of 9 × 9 × 9 for bulk $Ni_3S_2$. Then $Ni_3S_2$ (-111) surface was obtained by cutting from the optimized bulk $Ni_3S_2$ and was expanded into 2 × 2 supercell, with vacuum slabs larger than 15 Å along the z-axis. The Ni-rich $Ni_3S_2$ (-1 1 1) surface was confirmed as the most stable termination of (-1 1 1) facet that is likely to be experimentally realized based on previous calculations.[7] The 5-coordinated Ni atom on surface was replaced by a Cu atom to construct the Cu-doped $Ni_3S_2$ (-1 1 1) surface. The 3 × 3 × 1 K-point mesh was applied for geometry optimizations of $Ni_3S_2$ (-1 1 1) surfaces. The H atom was then put on the different sites of the optimized surfaces.

According to the computational hydrogen electrode (CHE) model,[8] the chemical potential of a proton−electron pair at 0 V (vs RHE) is defined equal to one half of the chemical potential of molecular hydrogen at all temperatures and $1.01 \times 10^5$ Pa, namely, $H^+ + e^- = 1/2H_2$. Then the Gibbs free energy of hydrogen adsorption ($\Delta G_H$) is computed as a criterion of HER catalytic activity, which is defined as:

$$\Delta G_H = E_{ads}(H^*) + \Delta ZPE - T\Delta S_H \quad (1)$$

where $E_{ads}(H^*)$ is the adsorption energy of hydrogen atom, ΔZPE is the zero-point energy change of adsorbed H against free H atom, and $\Delta S_H$ is the entropy difference between H* and free H atom at room temperature (298.15 K). As a benchmark, the computed $\Delta G_H$ value on the Pt surface is −0.09 eV.[9] According to the Sabatier principle,[9] a smaller $|\Delta G_H|$ value means the higher HER activity for the surface.

The barrier of water dissociation on $Ni_3S_2$ (-1 1 1) surface and Cu-doped $Ni_3S_2$ (-1 1 1) surface was performed by climbing-image nudged elastic band (CI-NEB) method implemented in VASP.[10] The transition states were determined by relaxing the force below 0.05 eV/Å.

## 3. Figures:

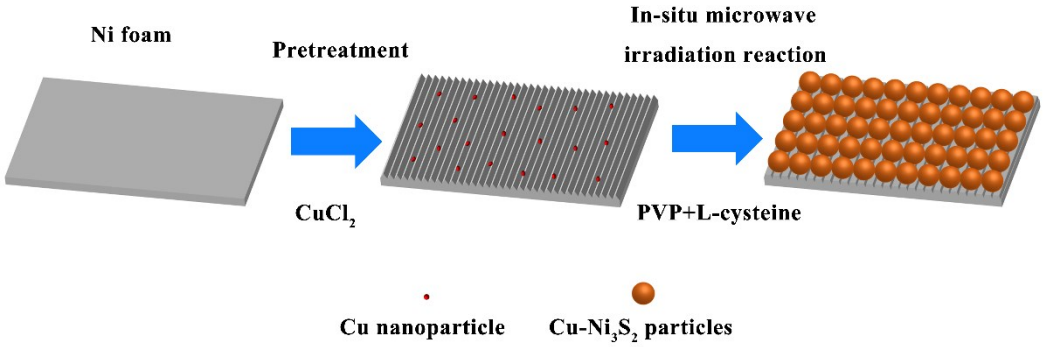


**Figure S1** Schematic illustration of the fabrication process of Cu-$Ni_3S_2$ nanoparticles

**Calibration of SCE electrode**

Before electrochemical measurements, the SCE electrode was calibrated in 1 M KOH and 1 M PBS with two Pt wires as working and counter electrodes and SCE as reference electrode. The electrolytes were purged using pure $H_2$. LSV tests were carried out at scan rate of 0.1 mV $s^{-1}$. The potentials correspond to current value of 0 mA on the LSV curves are the thermodynamic potential for hydrogen electrode reaction. The potentials are -1.041 V in 1 M KOH and -0.62 V in 1 M PBS, as shown in Figure S2. As a result, the E(RHE) can be expressed as:

$$E(RHE)=E(SCE)+1.041\ V \quad \text{(in 1 M KOH)} \qquad (2)$$

$$E(RHE)=E(SCE)+0.62\ V \quad \text{(in 1 M PBS)} \qquad (3)$$

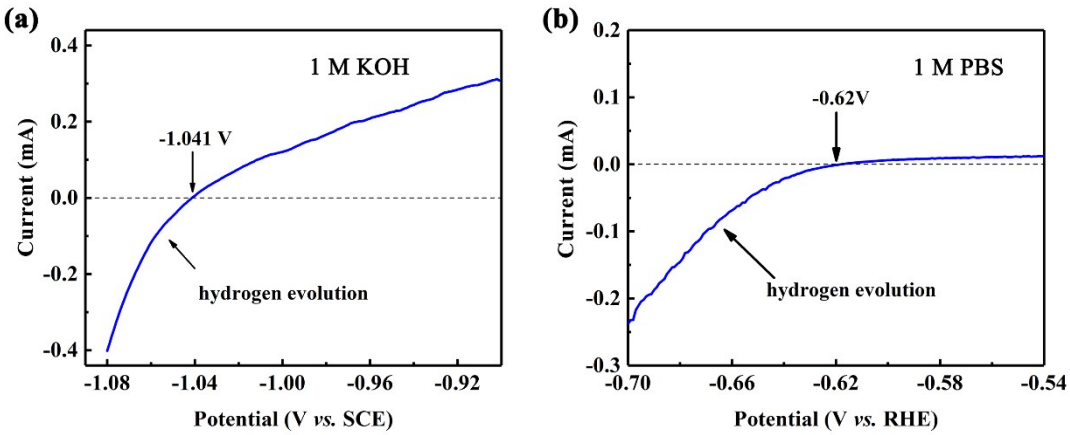


**Figure S2** LSV curve for the SCE calibration in 1 M KOH (a) and 1 M PBS (b), respectively.

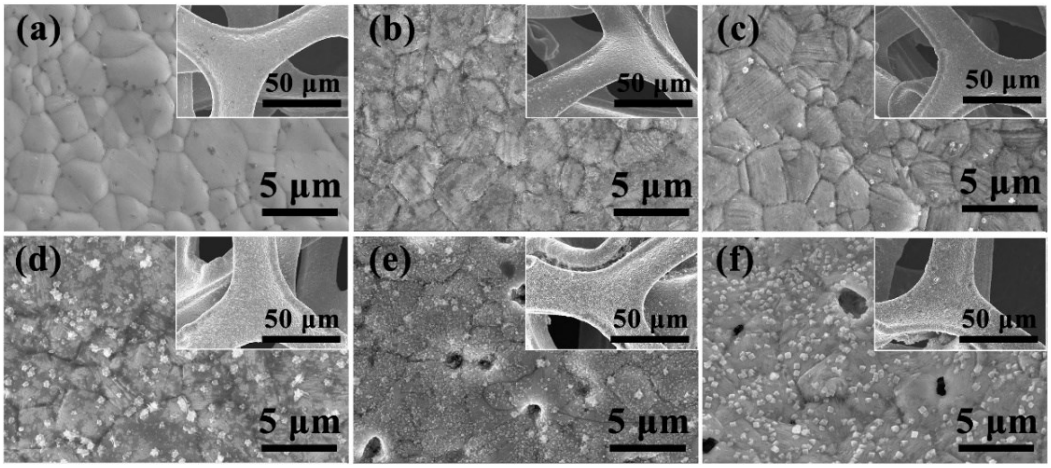


**Figure S3** Surface morphology of pristine Ni foam (a) and Ni foams pretreated in $CuCl_2$ solution for 2min (b), 4 min (c), 6 min (d), 8min (e), and 10 min (f), respectively, the insets are the corresponding surface morphology at low magnification.

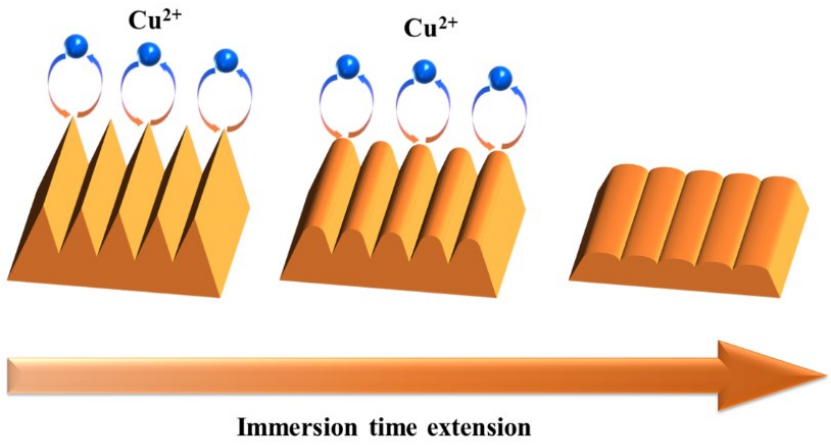


**Figure S4** Schematic illustration of the "point-effect" of Ni foam immersed in $CuCl_2$ with extra-long time (8 and 10 min).

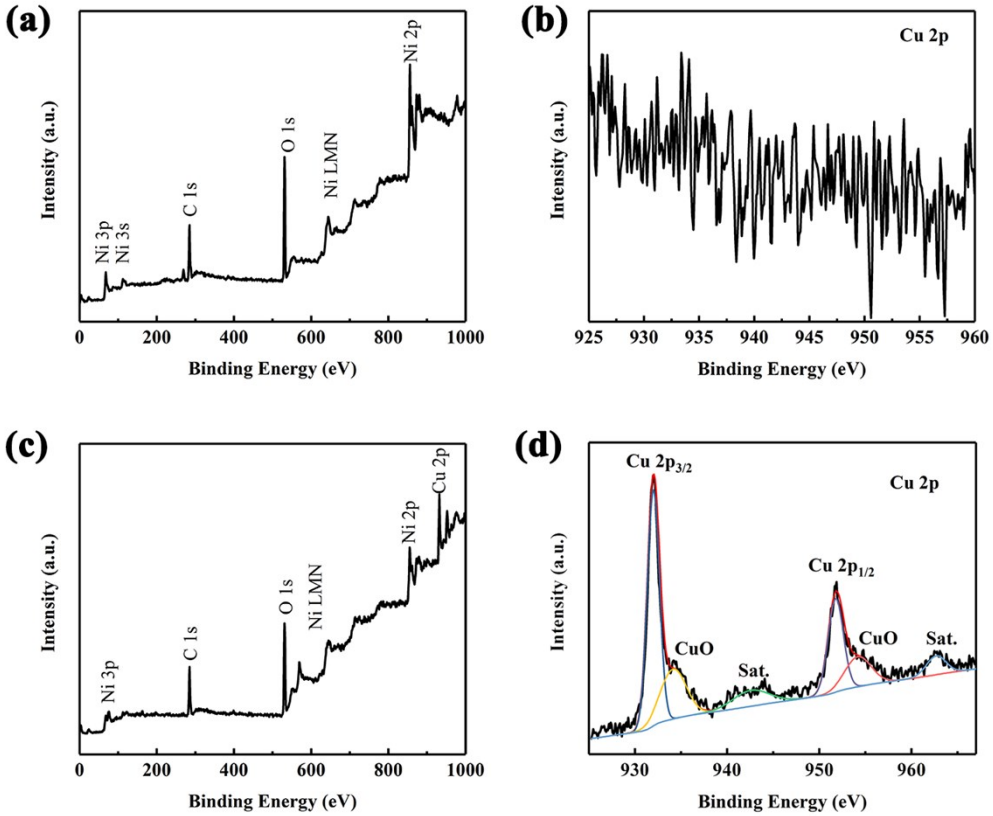


**Figure S5** XPS spectra of pristine Ni foam: (a) survey and (b) Cu *2p* spectra; XPS spectra of Ni foam pretreated in $CuCl_2$ solution for 6 min: (c) survey and (d) Cu *2p* spectra.

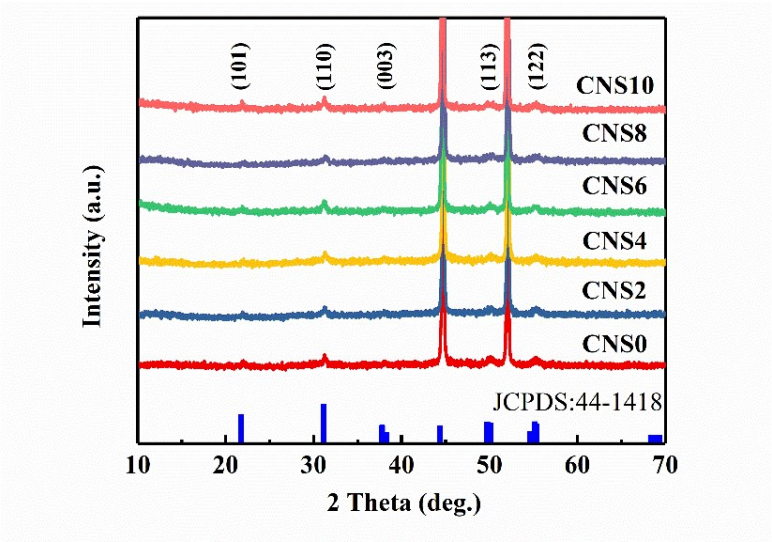


**Figure S6** XRD patterns of CNS0, CNS2, CNS4, CNS6, CNS8 and CNS10, respectively.

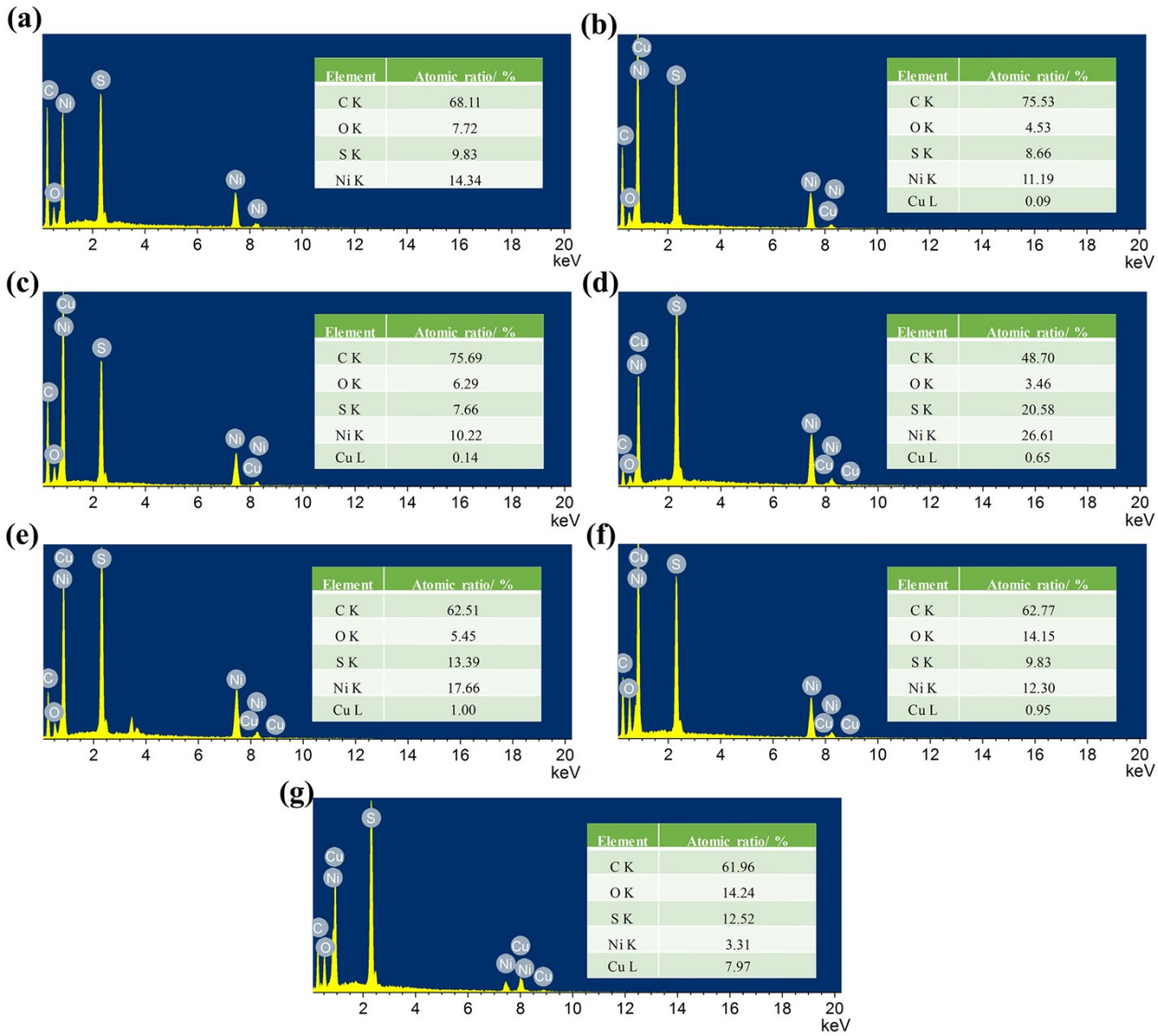


**Figure S7** EDX spectra of the catalysts: (a) CNS0, (b) CNS2, (c) CNS4, (d) CNS6, (e) CNS8, (f) CNS10, and (G) Cu-rich area in CNS10. The insets are the corresponding atomic ratio of each sample.

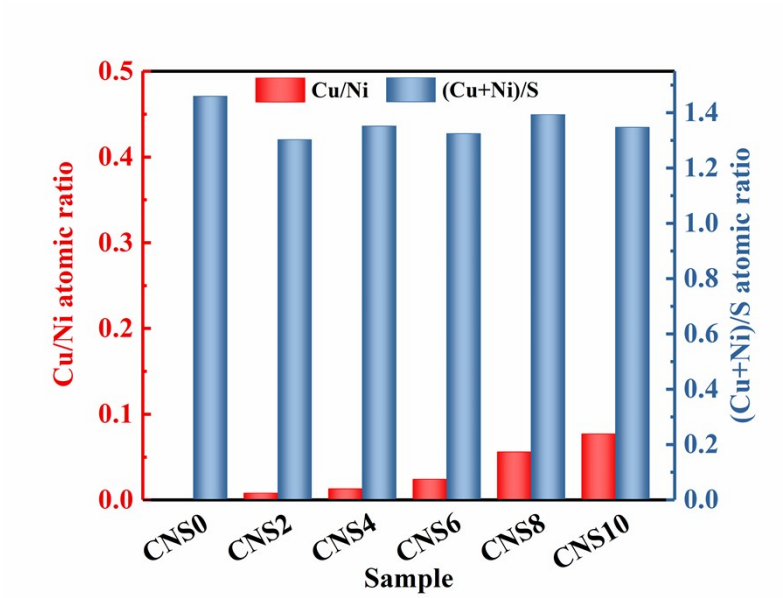


**Figure S8** Cu/Ni and (Cu+Ni)/S atomic ratio of CNS0, CNS2, CNS4, CNS6, CNS8 and CNS10, respectively.

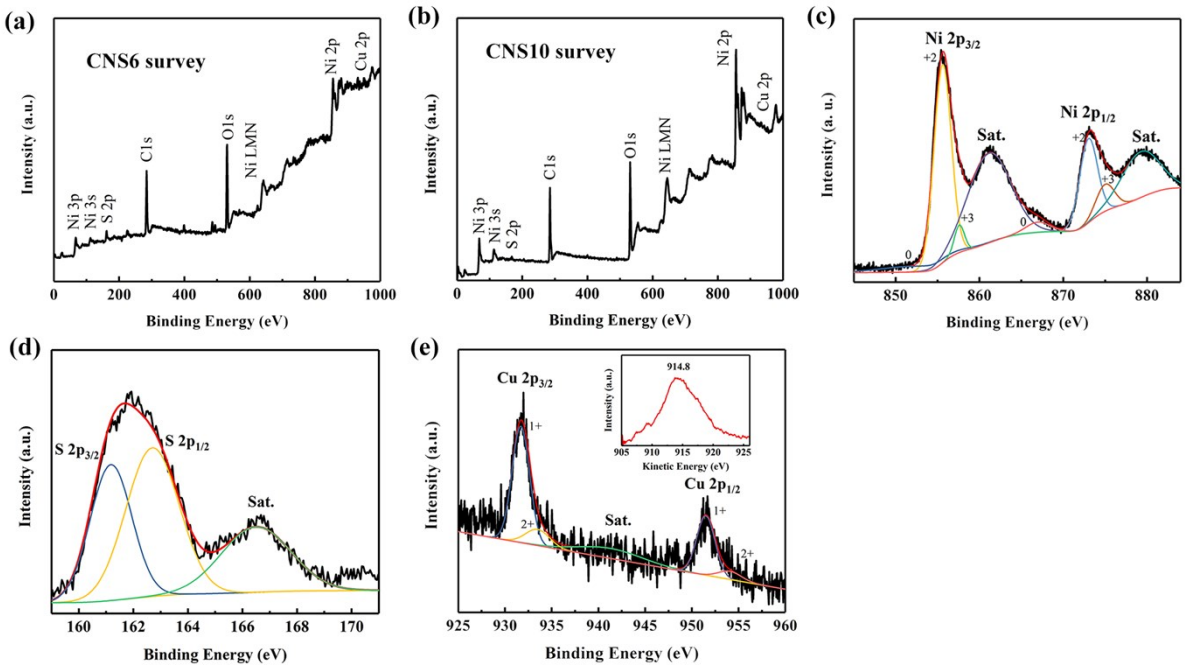


**Figure S9** (a) XPS survey spectrum of CNS6, XPS spectra of CNS10: (b) survey spectrum, (c) Ni 2p spectrum, (d) S 2p spectrum, and (e) Cu 2p spectrum. The inset in (e) is the Cu LMM spectrum.

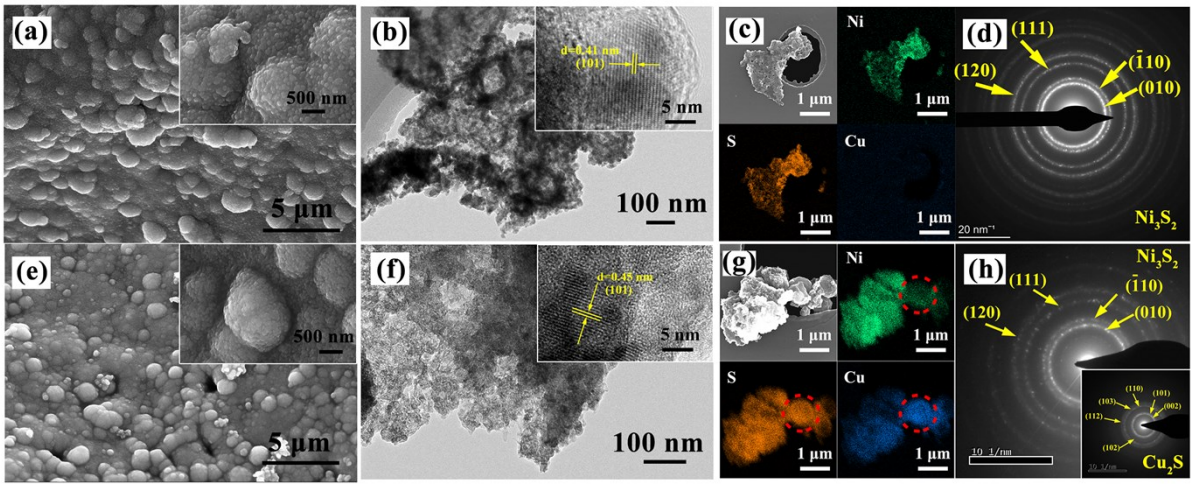


**Figure S10** The SEM (a), TEM (b) images, EDS mapping (c) and SAED pattern(d) of CNS0; The SEM (e), TEM (f) images, EDS mapping (g) and SAED pattern (h) of CNS10. The insets in (a) and (e) are the corresponding magnified SEM images, the insets in (b) and (f) are the corresponding HRTEM images.

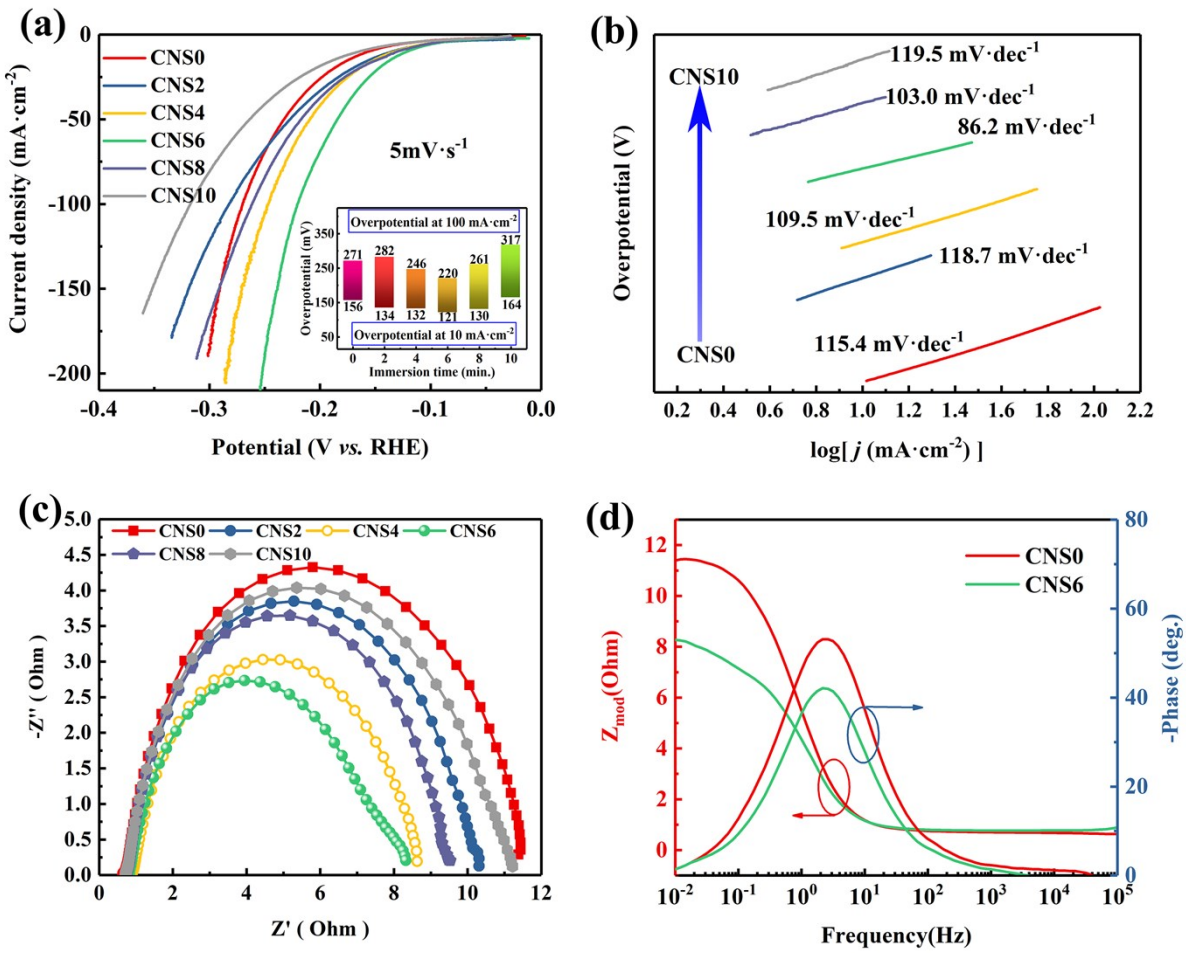


**Figure S11** HER performance of CNS0, CNS2, CNS4, CNS6, CNS8 and CNS10 in 1M KOH. (a) LSV curves, (b) Tafel plots, (c) Nyquist plots recorded at overpotential of 200 mV in 1 M KOH electrolyte and (d) Bode plots of CNS0 and CNS6 recorded at the same condition with the Nyquist plot. The inset in (a) is the overpotentials at 10 and 100 mA $cm^{-2}$.

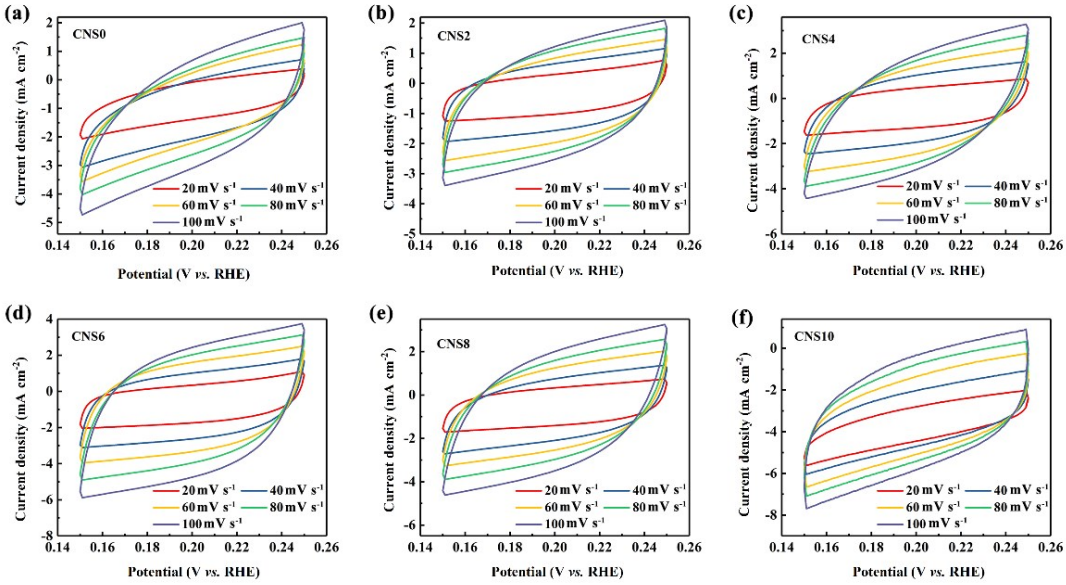


**Figure S12** CV curves of CNS0, CNS2, CNS4, CNS6, CNS8 and CNS10 recorded in the potential range of 0.15-0.25 V *vs*. RHE with different scan rates in 1M KOH, respectively.

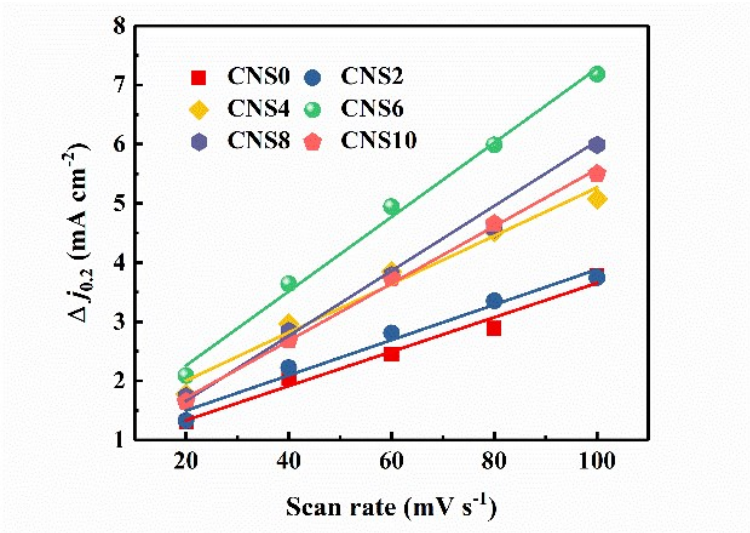


**Figure S13** Current density differences at 0.2V (*vs*. RHE) of the CV curves as a function of scan rates for CNS0, CNS2, CNS4, CNS6, CNS8 and CNS10 in 1M KOH.

The corresponding EDLC values ($C_{dl}$) are obtained by 1/2 slops of the $\Delta j_{0.2}$ *vs.* scan rates[11]. The values are 11.1, 14.9, 20.4, 31.4, 27.4 and 24.2 mF cm$^{-2}$ for CNS0, CNS2, CNS4, CNS6, CNS8 and CNS10, respectively.

The electrochemical surface area (ECSA) of each sample is obtained as[12]:

$$\text{ECSA}=C_{dl}/0.04 \qquad (4)$$

where 0.04 is the $C_{dl}$ value of 0.04 mF cm$^{-2}$ for a smooth surface. The ECSA values are 277.5, 372.5, 510.0, 785.0, 685.0, 605.0 cm$_{\text{ECSA}}^{-2}$ for CNS0, CNS2, CNS4, CNS6, CNS8 and CNS10, respectively.

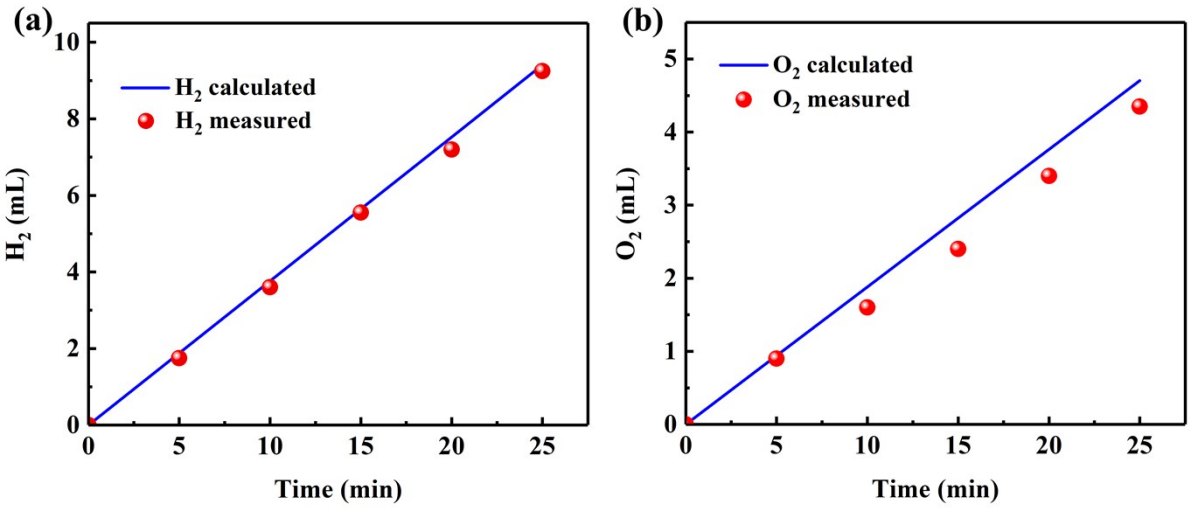


**Figure S14** Theoretical and practical $H_2$ (a) and $O_2$ (b) amount during the HER and OER process with applied constant 50 mA $cm^{-2}$ current density.

The Faradaic efficiency is obtained using the following equation:

$$FE=z\times n\times F/(I\times t)\times 100\% \quad (5)$$

where *FE* is the Faradaic efficiency, *z* is the electron transfer number, n is the amount (moles) of the gas generated during the HER or OER process, *F* is the Faradaic constant (96485.3 C $mol^{-1}$), *I* is the applied constant current (A), and *t* is the electrolysis time (s).

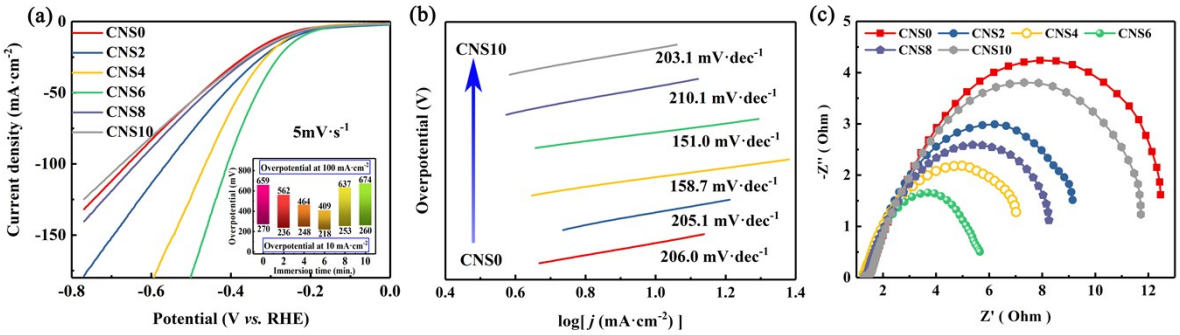


**Figure S15** HER performance of CNS0, CNS2, CNS4, CNS6, CNS8 and CNS10 in 1M PBS. (a) LSV curves, (b) Tafel plots and (c) Nyquist plots recorded at overpotential of 250 mV in 1 M PBS electrolyte. The inset in (a) is the overpotentials at 10 and 100 mA $cm^{-2}$.

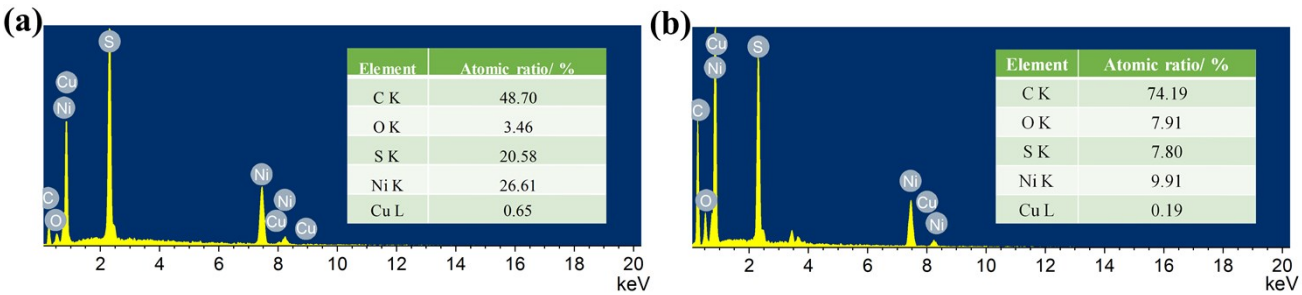


**Figure S16** EDX results of CNS6 before (a) and after (b) the 2000 continuous LSV measurements in 1M KOH. The insets show the atomic ratio for each spectrum.

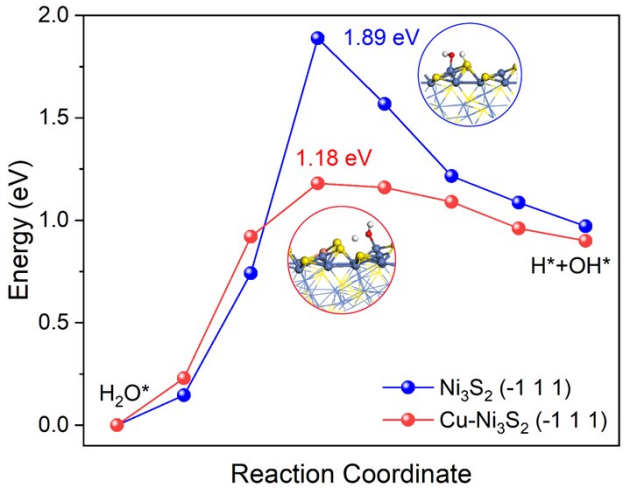


**Figure S17** The obtained minimum-energy pathways for $H_2O$ dissociation on $Ni_3S_2$ (-1 1 1) surface and Cu-doped $Ni_3S_2$ (-1 1 1) surface. The insets show the configurations of corresponding transition states.

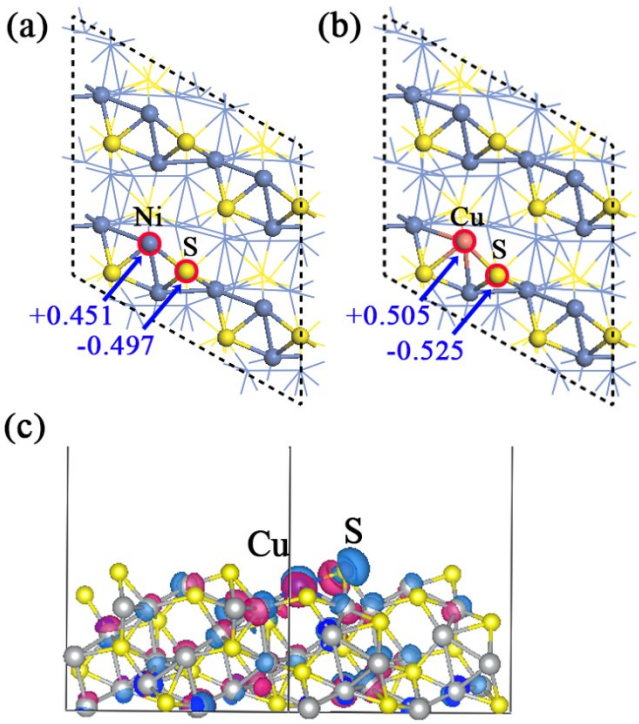


**Figure S18** (a) The Bader charge assigned on Ni atom and S atom on surface of $Ni_3S_2$ (-1 1 1), (b) The Bader charge assigned on Cu atom and S atom on surface of Cu-$Ni_3S_2$ (-1 1 1), (c) isosurface of electron density difference between $Ni_3S_2$ (-1 1 1) and Cu-doped $Ni_3S_2$ (-1 1 1). The color for electron depletion and electron accumulation region are blue and red, with the isovalue of 0.02 e/ $Å^3$.

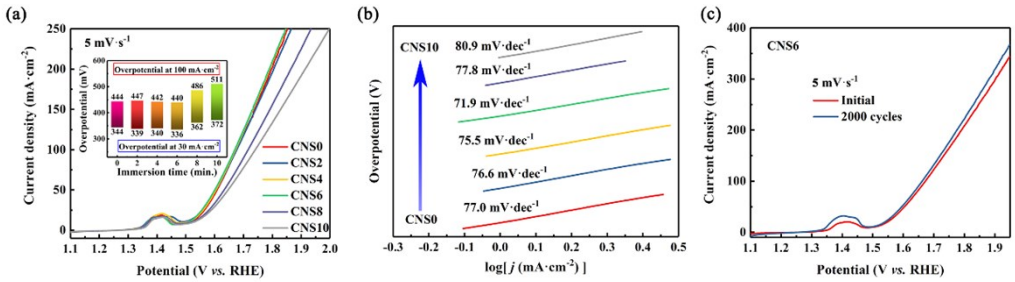


**Figure S19** OER performance of CNS0, CNS2, CNS4, CNS6, CNS8 and CNS10 in 1M KOH, respectively. (a) LSV curves, (b) Tafel plots and (c) LSV curves of CNS6 measured before and after 2000 cycles in 1 M KOH electrolyte.

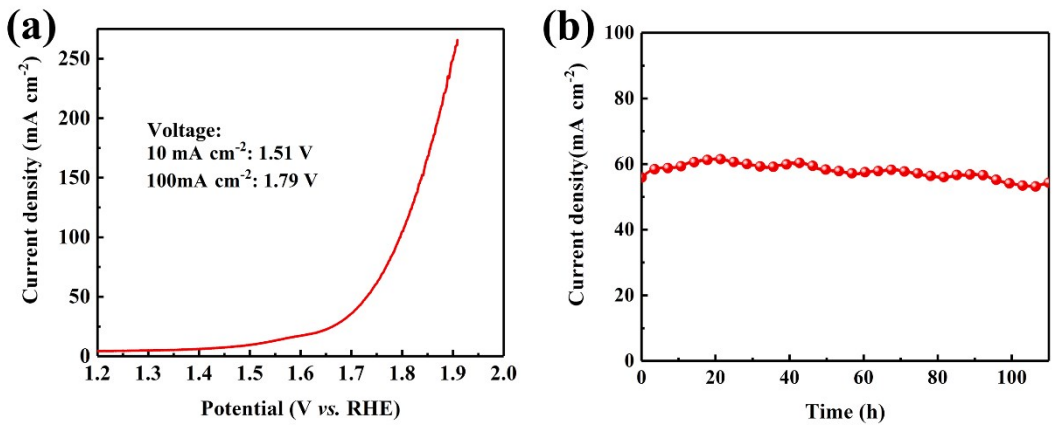


**Figure S20** LSV curve of the electrolyzer consisting of Cu-$Ni_3S_2$ as anode and cathode for overall water splitting in 1 M KOH solution (a), and the corresponding chronoamperometric curve at 1.74 V for 110 h (b).

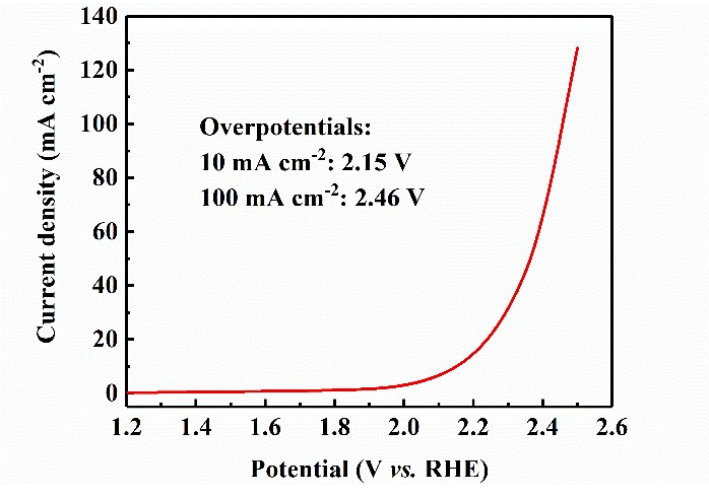


**Figure S21** LSV curve of CNS6 as anode and cathode for overall water splitting in 1 M PBS solution.

## 5. Tables

The weight of active materials can be calculated according to the reaction equation during the synthesis process:

$$2S^{2-} + 3Ni \rightarrow Ni_3S_2 \quad (6)$$

The weight increment of the Ni foams is induced by the incorporation of S into the Ni foams. So the masses of active materials ($m$) loaded on the Ni foams per square centimeter were calculated according to the as follows:

$$m = \Delta m \times 2M_{Ni3S2}/M_S \quad (7)$$

where $\Delta m$ represents the mass changes of Ni foams for per unit area of 1×1 $cm^2$ before and after the reaction. $M_S$ and $M_{Ni3S2}$ represent the molecular mass of S and $Ni_3S_2$. It should be noted that the weight of Cu is neglected, due to the very low content in the final active materials as shown in Figure S7. The results are shown in table R1.

**Table S1** Calculated mass of active materials loaded on nickel foams for CNS0, CNS2, CNS4, CNS6, CNS8 and CNS10. In order to make the data more credible, the data in this table are the average value for 5 pieces NFs with length of 5 cm, width of 1cm and thickness of 0.5 mm, respectively.

| Sample | $m_b$(mg) | $m_a$(mg) | $\Delta m'$ (mg) | $\Delta m$(mg) | $m$(mg) |
|---|---|---|---|---|---|
| **CNS0** | 145.4 | 148.4 | 3.00 | 0.60 | 2.25 |
| **CNS2** | 144.9 | 148.4 | 3.50 | 0.70 | 2.63 |
| **CNS6** | 140.4 | 143.6 | 3.20 | 0.64 | 2.40 |
| **CNS8** | 141.6 | 144.7 | 3.10 | 0.62 | 2.33 |
| **CNS10** | 137.5 | 141.1 | 3.60 | 0.72 | 2.70 |

$m_b$ is the weight of nickel foam before deposition.

$m_a$ is that of nickel foam after deposition. For these two parameters, two samples were used to verify the data.

$\Delta m'$ is the average value of the differences between $m_b$ and $m_a$ for the nickel foams with length of 5 cm, width of 1cm and thickness of 0.5 mm, respectively.

From table R1, the weight of active materials loaded on the NFs for per unit area (1×1 $cm^2$) is around 2~3 mg for all samples.

**Table S2** Comparison of the HER activity between CNS6 in this work and other $NiS_x$ based electrocatalysts in 1 M PBS reported previously.

| Electrocatalyst | Overpotential at 10 mA $cm^{-2}$ (mV) | Time for fabrication | Ref. |
|---|---|---|---|
| Cu-$Ni_3S_2$ NPs | 218 | 10 min | This work |
| $Ni_3S_2/Ni_2P$ NRs | 204 | 20 min | [13] |
| $NiS_2/MoS_2$/rGO | 229 | >8 h | [14] |
| $NiS_2$ NSs | 243 | 11h | [15] |
| $Ni_3S_2$ NSs | 220 | 10 h | [16] |

NPs=Nanoparticles NRs=Nanorods

NSs=Nanosheets

**Table S3** Detailed computational values of $E_{ads}$ (H*), ΔZPE, ΔTS and $\Delta G_H$ on different adsorption sites of $Ni_3S_2$ (-1 1 1) and Cu-$Ni_3S_2$ (-1 1 1) surface.

| | site | $E_{ads}$ (H*) | ΔZPE | ΔTS | $\Delta G_H$ |
|---|---|---|---|---|---|
| $Ni_3S_2$ (-1 1 1) | S | -0.193 | 0.223 | -0.186 | 0.080 |
| | Ni | 0.237 | 0.167 | -0.173 | 0.442 |
| Cu-$Ni_3S_2$ (-1 1 1) | S1 | -0.221 | 0.223 | -0.185 | 0.052 |
| | S2 | -0.199 | 0.223 | -0.186 | 0.075 |
| | Cu | 0.631 | 0.151 | -0.163 | 0.810 |
| | Ni | -0.707 | 0.171 | -0.177 | -0.495 |

**Table S4** Comparison of the overall water splitting performance between CNS6 in this work and other $Ni_3S_2$ based electrocatalysts reported previously.

| Electrocatalysts | Overpotential | | Ref. |
|---|---|---|---|
| | 10 mA $cm^{-2}$ | 100 mA $cm^{-2}$ | |
| Cu-$Ni_3S_2$ NPs | 1.51 | 1.79 | This work |
| $Ni_xCo_{3-x}S_4/Ni_3S_2$ NSs | 1.53 | 1.8 | [17] |
| $Ni_3S_2$ NSs | 1.76 for 13 mA $cm^{-2}$ | - | [18] |
| CuNiS NWs | 1.54 | - | [19] |
| Fe-$Ni_3S_2$ NSs | 1.54 | 1.7 | [20] |
| $MoS_2/Ni_3S_2$ NPs | 1.56 | - | [21] |
| $MoS_2$-$Ni_3S_2$ NRs | 1.5 | - | [22] |
| $Mo_x$-$Ni_3S_2$ MSs | 1.45 | 1.71 | [23] |

NPs=Nanoparticles NSs=Nanosheets

NWs=Nanowires NRs=Nanorods

MSs=Microspheres

**References**


[1] G. Kresse, J. Furthmüller, *Phys. Rev. B* **1996**, 54, 11169.

[2] P. E. Blöchl, *Phys. Rev. B* **1994**, 50, 17953.

[3] J. P. Perdew, K. Burke, M. Ernzerhof, *Phys. Rev. Lett.* **1996**, 77, 3865.

[4] S. Grimme, J. Antony, S. Ehrlich, H. Krieg, *J. Chem. Phys.* **2010**, 132, 154104.

[5] A. D. Vershinin, E. N. Selivanov, R. I. Gulyaeva, N. I. Sel'menskikh, *Inorg. Mater.* **2005**, 41, 882.

[6] H. J. Monkhorst, J. D. Pack, *Phys. Rev. B* **1976**, 13, 5188.

[7] T. Kou, T. Smart, B. Yao, I. Chen, D. Thota, Y. Ping, Y. Li, *Adv. Energy Mater.* **2018**, 8, 1703538.

[8] J. K. Nørskov, J. Rossmeisl, A. Logadottir, L. Lindqvist, J. R. Kitchin, T. Bligaard, H. Jónsson, *J. Phys. Chem. B* **2004**, 108, 17886.

[9] Y. Ouyang, C. Ling, Q. Chen, Z. Wang, L. Shi, J. Wang, *Chem. Mater.* **2016**, 28, 4390.

[10] G. Henkelman, B.P. Uberuaga, H. Jonsson, *J. Chem. Phys* **2000,** 113, 9901.

[11] C. Yang, M. Y. Gao, Q. B. Zhang, J. R. Zeng, X. T. Li, A. P. Abbott, *Nano Energy* **2017**, 36, 85.

[12] L. Zhuang, Y. Jia, H. Liu, X. Wang, R. K. Hocking, H. Liu, J. Chen, L. Ge, L. Zhang, M. Li, C.L. Dong, Y.C. Huang, S. Shen, D. Yang, Z. Zhu, X. Yao, *Advanced Materials* **2019**, 31, 1805581.

[13] Y. Zhou, T. Li, S. Xi, C. He, X. Yang, H. Wu, *CHEMCATCHEM* **2018**, 10, 5487.

[14] L. Wang, T. Guo, S. Sun, Y. Wang, X. Chen, K. Zhang, D. Zhang, Z. Xue, X. Zhou, *Catalysis Letters* **2019**, 149, 1197.

[15] C. Tang, Z. Pu, Q. Liu, A. M. Asiri, X. Sun, *Electrochimica Acta* **2015**, 153, 508.

[16] C. Tang, Z. Pu, Q. Liu, A. M. Asiri, Y. Luo, X. Sun, *International Journal of Hydrogen Energy* **2015**, 40, 4727.

[17] Y. Wu, Y. Liu, G.-D. Li, X. Zou, X. Lian, D. Wang, L. Sun, T. Asefa, X. Zou, *Nano*

*Energy* **2017**, 35, 161.

[18] L.L. Feng, G. Yu, Y. Wu, G.D. Li, H. Li, Y. Sun, T. Asefa, W. Chen, X. Zou, *Journal of the American Chemical Society* **2015**, 137, 14023.

[19] D. Cao, D. Cheng, *Chemical Communications* **2019**, 55, 8154.

[20] G. Zhang, Y.-S. Feng, W.-T. Lu, D. He, C.Y. Wang, Y.K. Li, X.Y. Wang, F.F. Cao, *ACS Catalysis* **2018**, 8, 5431.

[21] J. Zhang, T. Wang, D. Pohl, B. Rellinghaus, R. Dong, S. Liu, X. Zhuang, X. Feng, *Angewandte Chemie International Edition* **2016**, 55, 6702.

[22] Y. Yang, K. Zhang, H. Lin, X. Li, H. C. Chan, L. Yang, Q. Gao, *ACS Catalysis* **2017**, 7, 2357.

[23] Y. Wu, G.D. Li, Y. Liu, L. Yang, X. Lian, T. Asefa, X. Zou, *Advanced Functional Materials* **2016**, 26, 4839.